Physics Letters A 377 (2013) 1150–1153

Contents lists available at SciVerse ScienceDirect

Physics Letters A

www.elsevier.com/locate/pla

Lensless imaging of nanoporous glass with soft X-rays

Joshua J. Turner [a,b,*], Johanna Nelson [a,c], Xiaojing Huang [a,d], Jan Steinbrener [a], Chris Jacobsen [a]

[a] Physics Department, Stony Brook University, Stony Brook, NY 11794, United States
[b] Linac Coherent Light Source, SLAC National Accelerator Laboratory, Menlo Park, CA 94025, United States
[c] Stanford Institute for Materials and Energy Science, SLAC National Accelerator Laboratory, Menlo Park, CA 94025, United States
[d] National Synchrotron Light Source II, Brookhaven National Laboratory, Upton, NY 11973, United States

ARTICLE INFO

Article history:
Received 28 December 2012
Accepted 4 February 2013
Available online 19 February 2013
Communicated by V.M. Agranovich

Keywords:
Coherence
X-ray scattering
Phase retrieval
Nanoporosity

ABSTRACT

Coherent soft X-ray diffraction has been used to image nanoporous glass structure in two dimensions using different methods. The merit of the reconstructions was judged using a new method of Fourier phase correlation with a final, refined image. The porous structure was found to have a much larger average size then previously believed.

1. Introduction

Nanoporosity is an important characteristic to control in tailoring materials for specific functionalities, such as adjusting the internal surface area for catalysis and percolation. A major limiting factor in many studies of nanoporosity is the ability to characterize these types of materials appropriately. Important contributions are needed in imaging these types of structures over large sample volumes, at high resolution, and with sufficient efficiency. X-ray diffraction microscopy (XDM), also known as coherent diffraction imaging (CDI), has the ability to address these concerns [1]. The high penetrating power of X-rays allows one to observe structure over large volumes that is not accessible with other techniques. Furthermore, by obtaining an image from a continuous X-ray diffraction pattern, the resolution is not limited by the numerical aperture of present-day X-ray lenses and, for sufficiently robust specimens, there is no fundamental limit to approaching the wavelength limit in spatial resolution through the use of iterative, phase-retrieval algorithms. An additional, though less well-known benefit, is the efficiency where for radiation-sensitive specimens, such as those found in biology [2] or even magnetism [3], the elimination of the inefficient X-ray lens is important for achieving a higher spatial resolution for a given X-ray exposure [4].

Improved methods are needed to perform imaging studies in a 'single-shot' environment, such as those used at X-ray free electron laser (FEL) facilities [5], which usually consists of measuring isolated particles in a plane-wave geometry [6]. For instance, the ultra-fast morphology of the nanoporous structure would be able to be mapped out under different conditions, such as with controlled shock waves [7] or THz laser illumination for pulsed, high electric-field exposure [8]. An important part of these studies is to compare the reconstructions adequately, either between images of different particles assumed to be the same, or using the same sample after changes are induced through external stimuli.

In this Letter, we use a new method of comparing reconstructions by using the recovered Fourier phases as a metric. We demonstrate this by the imaging of nanoscale porous glass in two dimensions and find the pore sizes to differ than what was expected by as much as about an order of magnitude. By reconstructing multiple images of the same glass object in parallel over about a 24 hour period, we compare them to a baseline reconstruction of the porous structure through the reconstructed phase in reciprocal space. Since getting an idea of mesoscopic structure soon after data collection is important for industrial applications such as in catalysis studies, this could be used to collect large statistics of nanoporous particles and compare the results in a timely manner.

2. Material and methods

The sample studied was nanoporous glass, also known as *thirsty* glass for its large absorptive capacity. Though composed mostly of

* Corresponding author at: Linac Coherent Light Source, SLAC National Accelerator Laboratory, Menlo Park, CA 94025, United States.
E-mail address: joshuat@slac.stanford.edu (J.J. Turner).

0375-9601/$ – see front matter
http://dx.doi.org/10.1016/j.physleta.2013.02.005

SiO_2, it also contains 3% B_2O_3 and less than a percent of Na_2O. The sample has an open cell pore structure with characteristic cavity sizes of tens up to 200 Å [9]. As a result it is highly absorptive, with an internal surface area anywhere from 90–125 m^2/g of material [10] to 150 m^2/g [11] as measured by neutron diffraction and positron annihilation, respectively. The structure is commonly defined as bicontinuous and its porosity has been measured at $\sim$ 32–36% [10]. Samples were prepared by attaching particles diffusely to transparent films on TEM grids using the inherent surface adhesion, enabling X-ray illumination of single glass structures.

All the coherent X-ray diffraction measurements reported here were collected using a custom apparatus [12], though not presently in operation, at beamline 9.0.1 of the Advanced Light Source synchrotron facility, Lawrence Berkeley National Laboratory. This beamline uses a planar undulator to produce linearly polarized soft X-rays, and a high throughput zone plate monochromator [13] operated at 750 eV with a resolving power of $\lambda/\Delta\lambda \simeq 700$. The pinhole used to monochromatize the dispersed radiation had a diameter $D = 5$ μm and gave a 20 μm transverse coherence length at the sample, which was placed in the far-field. A backside-thinned CCD detector (Roper Scientific MTE-2) with 1340×1300 pixels of 20 μm pixel size was located 18 cm downstream of the particle, with a scatter guard in between the two. A 1 mm movable beamstop is also used upstream of the camera to prevent saturation by blocking the strong, low-frequency signal. For a given projection of the sample, we recorded 60 different exposures, including background images. These are taken with a range of acquisition times anywhere from 1 ms up to 30 s and are assembled into a single, total diffraction pattern. This mode of data collection is conducted to maximize signal-to-noise for different spatial frequency ranges for each exposure, a consequence of the limitation of dynamic range of the direct-detection CCD.

3. Results and discussion

Complex-valued nanoporous glass was phased by three independent investigators to demonstrate the method of reconstructed Fourier phase correlation. The initial reconstructions were performed simultaneously and used different methods and incorporated different procedures of data assembly. All calculations were performed on standard laptop CPUs, two within 24 hours and the third within 48 hours after data collection. Though we describe this as rapid, the recent idea of utilizing GPUs [14] will speed this up substantially. The assembly of the 60 diffraction patterns was conducted either through individual manual assembly scripts, or new automatic software recently written for the purposes of high-volume speckle pattern assembly [15]. Combinations of two different algorithms were used along with different methods of finding the support constraint. The algorithms chosen were the difference map [16] and the hybrid input–output algorithm [17], a variation of the error-reduction algorithm originally developed by Gerchberg and Saxton in 1972 [18]. All supports were calculated using the autocorrelation of the Fourier plane intensities to find a first estimate in real-space, followed by fine adjustment through some combination of manual adjustment and the Shrinkwrap algorithm [19]. All computations were achieved by down-sampling the full speckle pattern by a factor of two as the data had a Whittaker–Shannon sampling of 20 [20]. The details of the methods used are summarized in Table 1.

Fig. 1 shows the complex images obtained by the various data processing procedures. All images had phase ramps removed, a global phase set between all reconstructions, and were high-pass filtered to soften the effect of the discontinuity from unconstrained reconstruction of low spatial frequency Fourier plane magnitudes obscured by the beamstop. Though there are noticeable differences between rapid reconstructions A–C, they are similar enough to identify the quality of and the main features of the specimen. Image D was not a rapid reconstruction and was completed using a careful refinement approach including: adjustment of the support as a function of the impact on the PRTF curve (described below) using Shrinkwrap [19], more averaging over initial random phases [21] and over a greater number of iterates [22], and closer monitoring of the difference-map error [16] to guide the final adjustments.

To check the merit of the final reconstruction and of the averaging procedure, we plot the phase retrieval transfer function (PRTF) in Fig. 2. This is the ratio of the magnitude of the average complex amplitude of the reconstruction in reciprocal space over the square root of the intensity measured [23], or of the modulus squared as it is more applicable to the modulation transfer function [22]. The magnitude of this ratio is plotted as a function of q, the magnitude of the momentum transfer $\mathbf{q} = \mathbf{k}_f - \mathbf{k}_i$ with $|k| = 2\pi/\lambda$. The PRTF remains above 0.5 for $q \leqslant 0.7$ nm^{-1}, and 0.35 up to $q = 0.5$ nm^{-1}, indicating the high fidelity of the original object as well as the

Table 1
Reconstruction methods.

Method	Algorithm[a]	Data[b]	Support[c]	$N_s : N_i$[d]
A	HIO	H	S	10 : 500
B	DM	C	M–S	10 : 500
C	DM	H	S–M	10 : 1000
D	DM	C	S–M	26 : 1000

[a] Difference map (DM) or hybrid input–output (HIO).
[b] Data assembly completed by individual scripts from hand-merged (H) or automatic [15] computational software (C).
[c] Calculated by Shrinkwrap (S) or manually (M), where the first listed was used more.
[d] Number of random starts: Number of iterations per start.

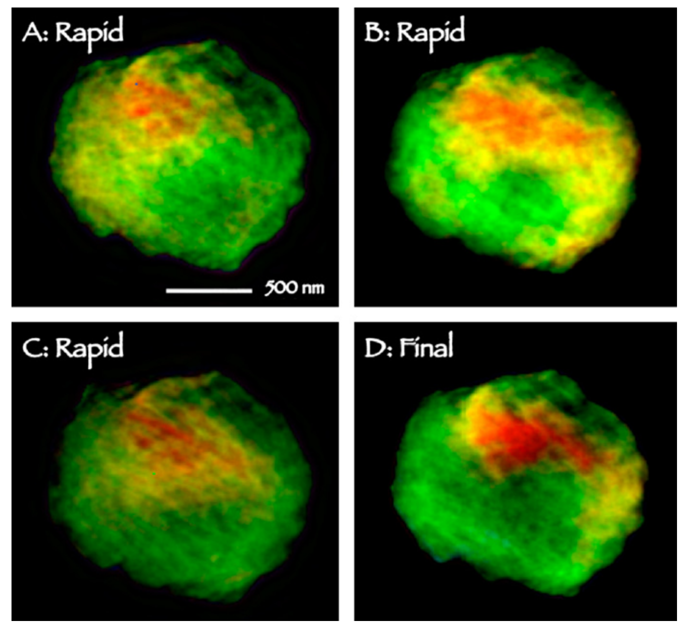

Fig. 1. Rapid reconstructions of a nanoporous glass particle from the same data using different methods. The three reconstructions A through C were performed independently at the time of data collection, and all were calculated using slightly different techniques, the details of which are summarized in Table 1. Each image is complex-valued, comprised of two components: brightness – which is proportional to the amplitude, or the inverse of electron absorption, and color – representing the phase distribution of the object in real-space, related to the X-ray dispersion. Image D is a reconstruction which was not performed at the time of data collection and was able to take advantage of more thorough reconstruction machinery. It serves as a gauge of how well the nanoglass objects were reconstructed. The structure seen in both components of the image is due to the thickness variation and porosity at the nanoscale.

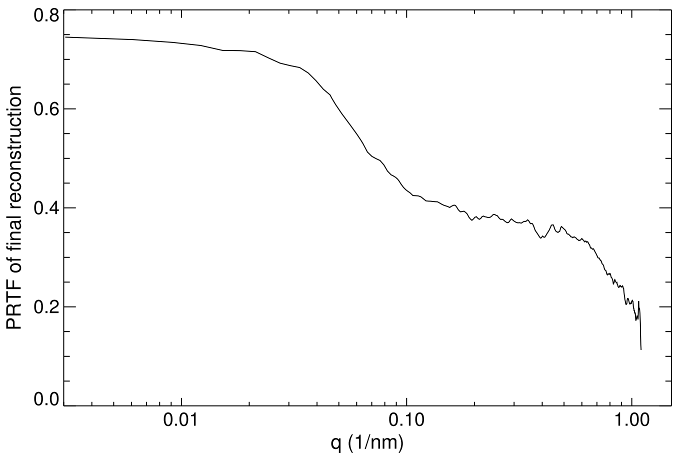

Fig. 2. A plot of the phase retrieval transfer function of the final reconstruction, panel D in Fig. 1. This is the ratio of the magnitude of the average complex amplitude of the reconstruction in reciprocal space to the square root of the intensity measured, and is plotted as a function of the magnitude of the difference of the final and initial photon wavevectors, $\mathbf{q} = \mathbf{k}_f - \mathbf{k}_i$.

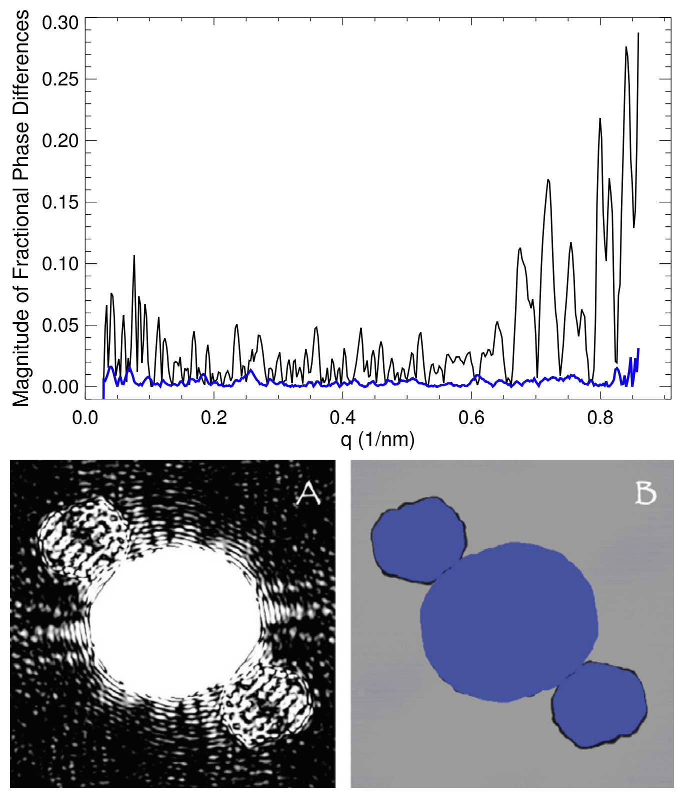

Fig. 3. A plot of the absolute value of Fourier phase differences. To understand how reliable the Fourier phases are retrieved, we calculate the absolute value of the difference between phases in the Fourier plane as a function of momentum transfer. The blue curve acts as the baseline, and is the Fourier phase difference between two of the final, average reconstructions. The black is the difference of the final image with rapid reconstruction C. Phases are reliably retrieved up to approximately $q = 0.6\ \text{nm}^{-1}$, or a spatial frequency $f = \theta/\lambda$ of about 47 μm^{-1}. Inset A – autocorrelation of the data. Inset B – the autocorrelation of the supports used for the final reconstruction (blue) overlayed on that used for the rapid reconstruction C (black) which were compared in the plot. (For interpretation of the references to color in this figure legend, the reader is referred to the web version of this Letter.)

high spatial resolution. The recovered pixel size is 10.3 nm, giving a total glass particle size over a micron.

To compare the rapidly recovered images, we describe a new relation between the reconstructed X-ray phases in Fourier space $\phi_{\mathcal{F}}(q)$ with the Fourier phase of the final reconstruction. This can be expressed with Fourier components according to the equation:

$$\delta\phi_{\mathcal{F}}(q) = A \int \Omega_d\, q^{d-1}\, dq \sum_{\alpha,\beta}^{N} \left|\phi_{\mathcal{F}}^{\alpha}(q) - \phi_{\mathcal{F}}^{\beta}(q)\right|$$

in d-dimensions, though in this work we are only displaying reconstructions in two dimensions, where $\Omega_d = 2\pi^{d/2}/\Gamma(\frac{d}{2}) = 2\pi$ since the definition of Euler's gamma function is $\Gamma(z) = \int_0^\infty e^{-x}x^{(z-1)}\,dx$. The limits of integration are $(q - \delta q/2, q + \delta q/2)$ for a resolution of δq and the normalization factor is

$$A = \frac{1}{\pi N(N-1)}$$

where N is the total number of images. These values are zero for images which have the exact same Fourier phase and are normalized such that a maximum possible difference gives unity. The curves in Fig. 3 show two such examples. The blue curve acts as the baseline, and is the Fourier phase difference between two final average reconstructions, each an average over 26 random starts. Note that these two averages used the same support, which would make the phase difference less at low frequencies than if one was altered with respect to the other. The black curve is the difference of the final image with rapid reconstruction C, judged to be the most inconsistent of the three by this method. Low frequency information below $q = 0.025\ \text{nm}^{-1}$ is where the beamstop is located and therefore is suppressed as it contains no information from measurable data. Using this Fourier method as a metric, we conclude that we can recover a reasonable, fairly accurate image between the different methods up to approximately $q = 0.6\ \text{nm}^{-1}$, or a spatial frequency $f = \theta/\lambda$ of about 47 μm^{-1} (or a half-period of 21 nm) over this time period of 24–48 hours, during extended X-ray data collection. Past this point, the average Fourier phases differ much more drastically.

The insets A and B in Fig. 3 show the autocorrelation of the data in real-space and the autocorrelation of the supports used for the two reconstructions in the plot, respectively. The blue autocorrelation is for the final reconstruction support and the black is for the rapid reconstruction C. It can be seen here that while an approximate first guess is easy to make under the right conditions, the support can be carefully refined. This takes more time, but can result in a better quality, final image. This can also be seen by calculating a similar comparison of the reconstructions in real space using the signal-to-noise cross-correlative method [4].

The level of similarity judged by this equation is enough to find that the porous structure is quite different than expected. The pores for this type of glass were formed to be 40 Å up to 200 Å, on average. In the reconstructions, we find an average pore size of about 50 nm, anywhere from a factor of two up to an order of magnitude larger than expected. Though this method does not have the spatial resolution to capture the smaller range of this expected pore distribution, we have found an average pore size which is much larger. To confirm this, we also analyzed the power spectral density curve, commonly measured in SAXS experiments though usually at much higher resolution, as shown in inset B of Fig. 4. A small enhancement of the intensity is found at 50 nm here is well, enlarged in the figure and shown with a power law fit. Lastly, we also compare with SEM images in inset A of Fig. 4, which can measure much finer resolution, though only at the surface of a large bulk glass sample. This finding outlines the need for new tools to study mesoscopic structure, particularly through larger volumes of materials. The next step to follow would be to study the structure of these types of nanoporous glass materials in three dimensions using coherent imaging techniques where one could directly answer the question on if these glasses display bicontinuity.

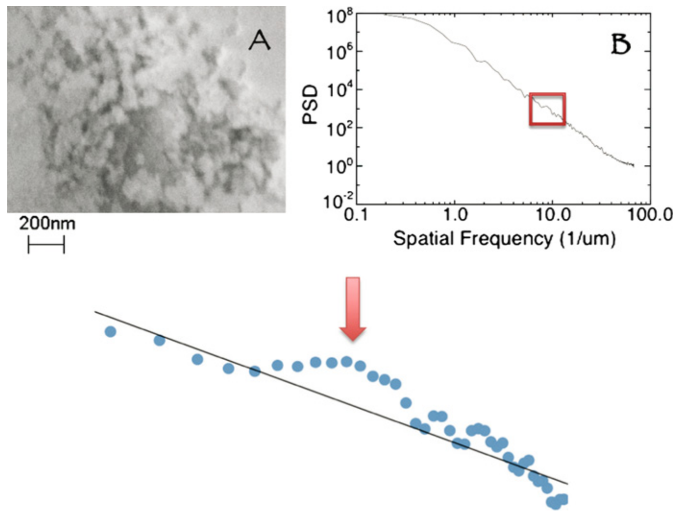

Fig. 4. A power law fit near the tail of the power spectra density curve showing a feature at 9 inverse microns, corresponding to 50 nm. This is consistent with the 50 nm scale features seen in the nanoporous glass reconstruction. Inset A: a large sample of the same nanoporous glass shown with a scanning electron micrograph. Though the electrons give a very high resolution spatial image, they can only resolve the nanoporosity on the top surface. The features seen on the surface of this bulk piece seem to agree with the 50 nm length scale seen in the reconstruction and from the power spectral density curve. Inset B: the full power spectral density of one of the rapid reconstructions.

In conclusion, we have used far-field coherent diffraction to invert and reconstruct soft X-ray speckle data from nanoporous glass to demonstrate a new relation to compare Fourier component phase differences, which will find use for single particle imaging, or ultra-fast mesoscopic structural changes in materials in X-ray FEL experiments. This could be highly useful in terms of a novel process for comparing material structure imaged though XDM and tailoring materials to obtain specific functionalities which might find use in an industrial setting. We found the pore structure to differ from the specifications they were originally grown for by as much as an order of magnitude.

Acknowledgements

We gratefully acknowledge D. Shapiro for help with some of the analysis and S. Boutet, J. Kirz, B. Larson, C. Holzner, and S. Marchesini for helpful discussions with this manuscript. The experiment was supported through the Division of Materials Sciences and Engineering, Office of Basic Energy Sciences, at the Department of Energy for support of X-ray diffraction microscopy methods and instrumentation development under contract DE-FG02-07ER46128.

References

[1] D. Sayre, Acta Crystallogr. 5 (1952) 843;
J.R. Fienup, Opt. Lett. 3 (1978) 27;
J.R. Fienup, Appl. Opt. 20 (1982) 2758;
J. Miao, P. Charalambous, J. Kirz, D. Sayre, Nature 400 (1999) 342.
[2] D. Shapiro, et al., PNAS 102 (2005) 15343;
X. Huang, et al., Phys. Rev. Lett. 103 (2009) 198101;
Y. Nishino, et al., Phys. Rev. Lett. 102 (2009) 018101;
J. Nelson, et al., PNAS 107 (2010) 7235.
[3] J.J. Turner, et al., Phys. Rev. Lett. 107 (2011) 033904;
A. Tripathi, et al., PNAS 10 (2011) 1073.
[4] X. Huang, et al., Opt. Expr. 17 (2009) 13541.
[5] P. Emma, et al., Nature Photon. 4 (2010) 641.
[6] M.M. Seibert, et al., Nature 470 (2011) 78.
[7] S.H. Glenzer, R. Redmer, et al., Rev. Mod. Phys. 81 (2009) 1625.
[8] M.C. Hoffmann, et al., Synchrotron Radiat. News 25 (2012) 17.
[9] Specifications supplied by Vycor brand porous glass 7930, manufactured by Corning Inc.
[10] M. Agamalian, J.M. Drake, S.K. Sinha, J.D. Axe, Phys. Rev. E 55 (1997) 3021.
[11] Y. Ito, T. Yamashina, M. Nagasaka, Appl. Phys. 6 (1975) 323.
[12] T. Beetz, et al., Nucl. Instrum. Methods Phys. Res. Sect. A 545 (2007) 459.
[13] M. Howells, et al., SPIE 4783 (2002) 65.
[14] D. Claus, et al., Opt. Expr. 20 (2012) 9911.
[15] J. Steinbrener, et al., Opt. Expr. 18 (2010) 18598.
[16] V. Elser, J. Opt. Soc. Amer. 20 (2003) 40.
[17] J.R. Fienup, Appl. Opt. 20 (1982) 2758.
[18] R.W. Gerchberg, W.O. Saxton, Optik 35 (1972) 237.
[19] S. Marchesini, et al., Phys. Rev. B 68 (2003) 140101.
[20] E.T. Whittaker, Proc. Roy. Soc. Edinburgh, Sect. A 35 (1915) 181;
C.E. Shannon, Proc. IRE 37 (1949) 10.
[21] J. Miao, et al., Phys. Rev. Lett. 97 (2006) 215503.
[22] P. Thibault, et al., Acta Crystallogr. Sect. A 62 (2006) 248.
[23] H. Chapman, et al., J. Opt. Soc. Amer. A 23 (2006) 1179.